Materials Today • Volume xxx, Number xx • xxxx 2024

ELSEVIER

Multi-effect coupling enhanced self-powered heterojunction ultraviolet photodetector with ultra-low detection limit

RESEARCH (LIGHT BLUE)

Mengji Dong [a,b], Xuemei Zheng [a,d], Qi Li [a,c], Yanli Liu [e], Xuan Di [e], Jianping Meng [a,b,*], Zhou Li [a,b,*]

[a] Beijing Institute of Nanoenergy and Nanosystems, Chinese Academy of Sciences, Beijing 101400, China
[b] School of Nanoscience and Engineering, University of Chinese Academy of Sciences, Beijing 100049, China
[c] College of Materials Science and Opto-Electronic Technology, University of Chinese Academy of Sciences, Beijing 100049, China
[d] College of Chemistry and Chemical Engineering, Guangxi University, Nanning 530004, China
[e] School of Engineering and Technology, China University of Geosciences (Beijing), Beijing 100083, China

Convenient, small-sized, and self-powered sensor units are easier to integrate, making them the future development direction of photodetectors. GaN materials with wide band gap are powerful candidates for UV detection, but most GaN based self-powered UV photodetectors have poor detection ability for the weak UV light, which limits their applications. This study reports a self-powered UV photodetector based on $BaTiO_3$/GaN heterojunction, which can detect ultra-weak UV light at a minimum of 0.68 nW/cm^2 by coupling the ferroelectric polarization, anti-reflection effect, and pyro-phototronic effect. The polarized $BaTiO_3$ thin film on the surface of GaN has an enhanced residual polarization field and generated anti-reflection effect, which can regulate the heterojunction band structure, suppress the dark current and minimize surface reflection of GaN. Simultaneously enhanced pyro-phototronic effect can significantly improve the response speed and responsivity of the device. The response time and recovery time of the device are as low as 8.794 ms and 5.018 ms. The maximum responsivity and detectivity are 88.206 mA/W and 7.392 $\times$ 10^{13} Jones, respectively, increased by 359% and 6065% compared to the device before polarization. Thanks to excellent material stability, the device has a sensitive and uniform response to continuously incident UV light. In addition, by simulating flame generation, it has been proven that the device has brilliant performance in flame detection and can achieve remote monitoring and fire warning functions. These results can promote the potential application of self-powered UV photodetectors based on $BaTiO_3$/GaN heterojunction in environmental monitoring and space communication fields.

Keywords: $BaTiO_3$/GaN heterojunction; UV photodetector; Self-powered; Flame detection

Introduction

Benefiting from the development of semiconductor science and nanotechnology, high-performance ultraviolet (UV) photodetectors have been widely used in fields such as biomedicine, environmental monitoring, industrial automation, fire monitoring, optical communication, astronomical studies and defense warning systems of military, etc [1–4]. The third-generation semiconductors such as silicon carbide (SiC), gallium nitride (GaN), zinc oxide (ZnO), diamond have the advantages of wide bandgap, high breakdown voltage, high thermal conductivity, high carrier

* Corresponding authors at: Beijing Institute of Nanoenergy and Nanosystems, Chinese Academy of Sciences, Beijing 101400, China.
E-mail addresses: Meng, J. (mengjianping@binn.cas.cn), Li, Z. (zli@binn.cas.cn).

 https://doi.org/10.1016/j.mattod.2024.03.004

Please cite this article in press as: M. Dong et al., Materials Today (2024), https://doi.org/10.1016/j.mattod.2024.03.004

mobility, and strong radiation resistance, have received extensive attention in the field of ultraviolet optoelectronics [2,5]. Among them, GaN has become a noteworthy candidate for UV light detection because of its wide direct band gap (~3.4 eV), mature production process and few material defects [6–8]. Many studies have proven that by structurally designing or surface modifying for GaN, UV photodetectors with high responsivity and ultra-fast response speed can be obtained [8–11].

However, it should be noted that in some special application scenarios, the intensity of UV is very weak, and only the UV photodetector with super detection ability can be competent. For example, a solar blind UV photodetector that detects flames needs to respond to light at an intensity of less than 1 nW/cm^2. Current equipment for ultra-low power UV detection mostly uses photomultiplier tubes or detects at large bias [12,13]. This makes photodetectors cumbersome and uneconomical, limiting their application [14]. Conversely, convenient, small-size, self-powered sensor units are easier to integrate, meeting the growing demand for intelligent, flexible, versatile, low-power photodetectors [1,15,16]. The development of small-size self-powered UV detectors is mostly based on p-n junctions, Schottky junctions and photoelectrochemical effects [14,17–19]. For example, Guo et al. constructed a GaN/Sn:Ga_2O_3 p-n junction UV photodetector [20]. Due to the powerful separation effect of photogenerated electron-hole pairs by the high built-in electric field, the device obtained a responsivity of up to 3.05 A/W and an ideal detectivity of 1.69×10^{13} Jones at zero bias. Polarized UV light detection is also of great significance in military applications [21]. Wu et al. constructed a 2D $PdSe_2$/GaN Schottky junction through in situ van der Waals growth [22]. The high-quality junction interface makes it have a fast and obvious UV response. The $PdSe_2$ layer is highly sensitive to polarized UV light, and the dichroic ratio of the device is as high as 4.5. Zhou et al. fabricated high-quality $CH_3NH_3PbCl_3$ ($MAPbCl_3$) thin films using a simple solution assisted halide exchange method [23]. The appropriate energy level alignment between $MAPbCl_3$ and adjacent charge transfer layers enables UV photodetector to operate in self-powered mode. A wearable UV monitoring wristband based on this self-powered UV photodetector can monitor indoor and outdoor ultraviolet radiation in all day. However, the poor detection ability of weak light has always been a major problem that limits the practical application of self-powered UV photodetectors [14,18]. Reducing dark current and enhancing light response are key to improving photodetector sensitivity [24]. Coupling multiple photoelectric effects is an effective way to solve this problem [25].

Previous works have proved that ferroelectric thin films can provide local electrostatic fields for semiconductors, suppress dark current, and enhance the detection ability of devices for weak light [26–28]. At the same time, the ferroelectrics themselves have pyroelectric effect, which can be combined with optoelectronic semiconductor to form a heterojunction. This can adjust the generation, separation, transport and recombination of photogenerated carriers, and significantly improve the responsivity, response speed and recovery speed of photodetectors [29,30]. The pyro-phototronic effect is a coupling effect of photoelectric effect and pyroelectric effect in semiconductor or ferroelectrics, which greatly improves the performance of photodetectors based on 2D PMA_2PbCl_4 MMB, $BaTiO_3$/GaN, 2D $(C_4H_9NH_3)_2(NH_2CHNH_2)Pb_2Br_7$, (n-hexylammonium)$_2CsPb_2Br_7$ [29,31–33]. As one of the most widely used ferroelectrics, $BaTiO_3$ (BTO) has a high residual polarization strength and pyroelectric coefficient [34,35]. Moreover, the destructive interference in the reflected light can be achieved through the film thickness design owing to the high transmittance and the low refractive index of $BaTiO_3$ thin film. $BaTiO_3$ thin film is an ideal anti-reflection film, which can reduce the reflection loss on the surface of semiconductor, thereby boosting the photon utilization of device [36].

In this work, we propose a self-powered UV photodetector for flame detection by coupling the ferroelectric polarization, anti-reflection effect, and pyro-phototronic effect (Fig. 1). This photodetector is based on the $BaTiO_3$/GaN (p-type) heterojunction structure, achieving a sensitive response to ultra-weak UV light with a power density of 0.68 nW/cm^2 and precise detection of flames. The anti-reflection effect is achieved through thickness design of $BaTiO_3$ thin film, successfully reducing the reflectivity of GaN surface to UV light by about 10%. Compared with unpolarized devices, the polarized $BaTiO_3$ thin film has a higher residual polarization intensity, suppressing the dark current of the device to around 5 pA, achieving 4.3×10^{13} Jones high detectivity. Simultaneously, the pyroelectric performance of the polarized ferroelectric thin film is significantly enhanced, and the photoelectric/thermoelectric synergistic response significantly improves the device's responsivity and response speed to UV light, enabling the device to accurately detect flames and provide early warning. The coupling effect of ferroelectric polarization and pyro-phototronic effect breaks the negative correlation coupling between responsivity and response speed, providing a new approach for the development of high-performance photodetectors.

Results and discussion

Design and characterization of $BaTiO_3$ thin film

The preparation process diagram of the device is shown in Fig. S1. $BaTiO_3$ thin film acts as an anti-reflection layer and generates a ferroelectric polarization field in the photodetector of $BaTiO_3$/GaN heterojunction, thereby improving the detection performance of the device. The characterization of $BaTiO_3$ thin film is shown in Fig. 2. $BaTiO_3$ thin film with a thickness of about 20 nm were prepared on GaN substrate by magnetron sputtering (Fig. S2). The bimodal in the X-ray diffraction (XRD) plot (Fig. 2a) is a typical characteristic peak of tetragonal $BaTiO_3$, which grows along the crystal plane orientation of (101) and (110) due to interfacial stress (Fig. S3) [34]. The cross-section high resolution transmission electron microscopy (HRTEM) image (Fig. 2b) of $BaTiO_3$ thin film shows that the film is a mixed phase of tetragonal phase and amorphous phase. The illustration shows an enlarged view of a certain tetragonal phase grain, with a crystal plane spacing of 0.2021 nm, which is consistent with the XRD test results. The element distribution diagram (Fig. S4) at the cross-section of $BaTiO_3$/GaN heterojunction is obtained by energy dispersive spectrometer (EDS), which proved the composition of $BaTiO_3$ thin film. Tauc plot (Fig. 2c) is obtained from the absorption data of $BaTiO_3$ thin film, and the calculated band gap

Please cite this article in press as: M. Dong et al., Materials Today (2024), https://doi.org/10.1016/j.mattod.2024.03.004

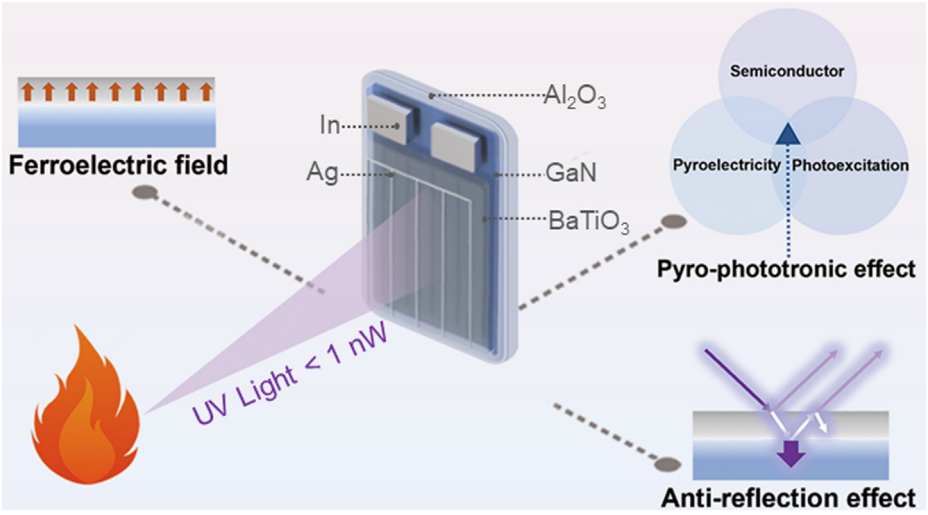

FIG. 1

A self-powered UV photodetector for flame detection by coupling ferroelectric field, anti-reflection effect, and pyro-phototronic effect.

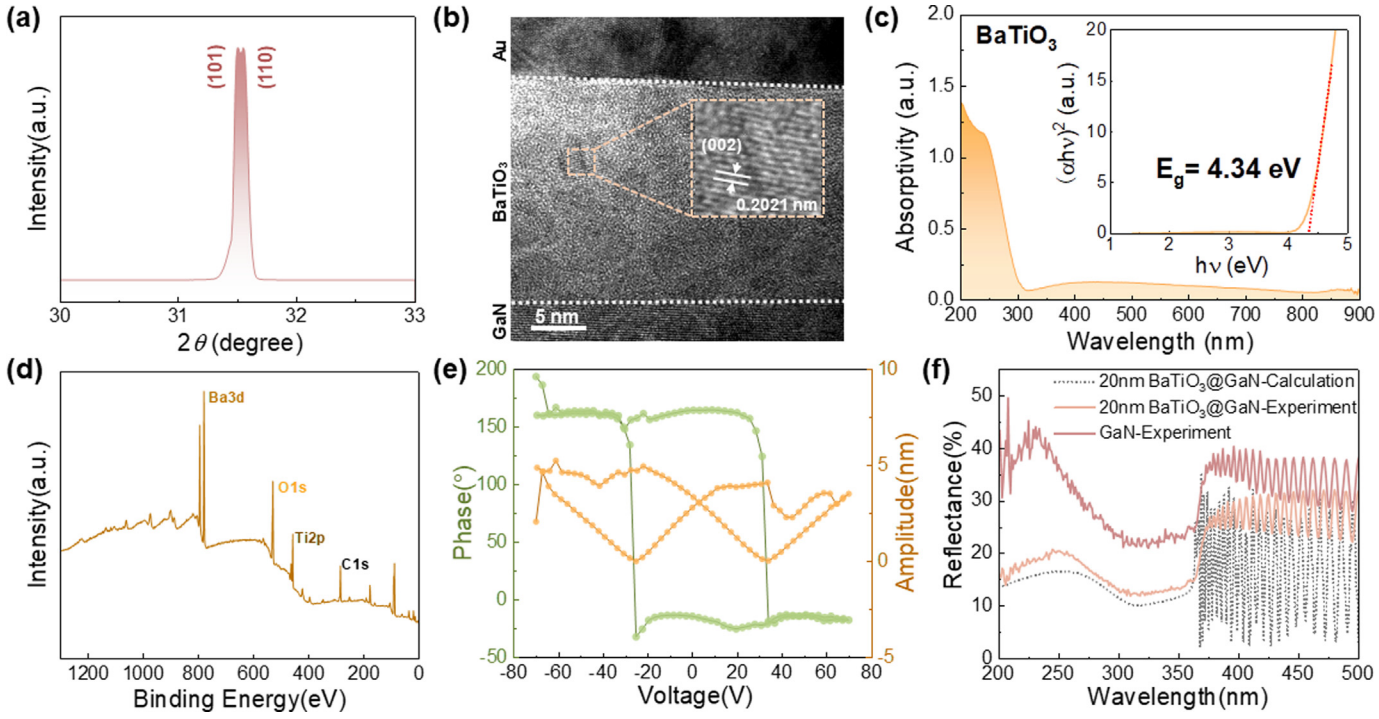

FIG. 2

Design and characterization of $BaTiO_3$ thin film. (a) Partial enlarged XRD pattern of $BaTiO_3$ thin film grown on GaN substrate. (b) HRTEM image of the cross-section of $BaTiO_3$ thin film grown on GaN substrate, the illustration shows an enlarged view of a certain tetragonal phase grain. (c) The absorption spectrum of $BaTiO_3$ thin film grown on amorphous SiO_2 substrate, the illustration shows the $(\alpha h\upsilon)^2$-$h\upsilon$ relationship curve obtained by Tauc Plot method. (d) XPS analysis spectrum of $BaTiO_3$ thin film. (e) Phase/amplitude-voltage function diagram of $BaTiO_3$ thin film grown on GaN substrate. (f) The experimental and fitting values of the reflectivity of $BaTiO_3$ thin film surface.

width of $BaTiO_3$ thin film is about 4.34 eV, which will not affect the absorption of UV light in the target band. The amorphous phases and the nanocrystalline lead to a blue shift in the light absorption edge of the thin film, resulting in a calculated band-gap value greater than the theoretical value (about 3.5 eV) [37,38]. X-ray photoelectron spectroscopy (XPS) is used to confirm the chemical states of elements in $BaTiO_3$ thin films. The peaks of binding energy at 779.96 eV, 529.82 eV, and

Please cite this article in press as: M. Dong et al., Materials Today (2024), https://doi.org/10.1016/j.mattod.2024.03.004

457.92 eV correspond to the chemical states of Ba3d, O1s, and Ti2p (Fig. 2d). In order to verify the ferroelectricity of $BaTiO_3$ thin films, piezoresponse force microscopy (PFM) is used to conduct a single point ferroelectricity test, and the standard amplitude butterfly curve and phase hysteresis curve were obtained (Fig. 2e). The phase change is about 180°, and the phase hysteresis curve has good rectangularity, indicating that the thin film has good ferroelectricity. Further, domain writing operations were carried out on the 20 μm*20 μm film surface to verify the ferroelectricity in micro regions (Fig. S5). The domain reading results shows that the ferroelectric domain had good overturning characteristics, and the spontaneous polarization direction of the thin films is perpendicular to the surface upward. The high reflectivity of GaN thin film surface to incident light can lead to significant light loss. $BaTiO_3$ thin film has high transmittance for UV light, and its refractive index is smaller than that of GaN thin film [36]. Through thickness design, ideal anti-reflection effect can be achieved. The refractive index and extinction coefficient of GaN and $BaTiO_3$ thin films are shown in Fig. S6. The design of a single-layer antireflection film is based on the principle of destructive interference (Fig. S7) [39]. Through TF Cala software, we fitted the ideal thickness of $BaTiO_3$ thin film. A 20 nm thick $BaTiO_3$ thin film can reduce the reflectivity of the GaN film surface by about 10% at wavelength from 200 nm to 375 nm (Fig. 2f). At 325 nm, $BaTiO_3$ thin film reduces the reflectivity of the device to incident light from 21% (bare GaN) to 12%, effectively reducing light loss. The slight deviation between the fitted device reflectivity data and the experimental data may be due to the uneven crystal phase and surface roughness of $BaTiO_3$ thin film.

Optoelectronic performance characterization of device

The structure and photoelectric performance of the device are shown in Fig. 3. Considering the surface area of the sample received light and the carrier collection efficiency, we prepared a strip silver electrode with a length of 8 mm and a width of 50 μm on a $BaTiO_3$ thin film by magnetron sputtering (Fig. 3a). Two indium electrodes were welded on the surface of the GaN film, and the I-V characteristic curve (Fig. S8) of the electrode and the GaN film as obtained to ensure that the indium electrode formed ohmic contact with the GaN film surface. The unpolarized device is in the fresh state (Fig. 3b i), the arrows in the figure represent randomly oriented ferroelectric domains. To enhance the ferroelectric field inside the $BaTiO_3$ thin film and achieve high suppression of dark current, the device is polarized using a high voltage of 7 kV (Fig. 3b ii), making the device into a polarization state. After polarization, the ferroelectric domain orientation in the $BaTiO_3$ thin film tends to be consistent, achieving polarization in the vertical direction of the thin film. The logarithmic I-V curve of the device under dark and UV light were obtained to verify the modulation of the ferroelectric field on the photoelectric performance of the device (Fig. 3b iii). After

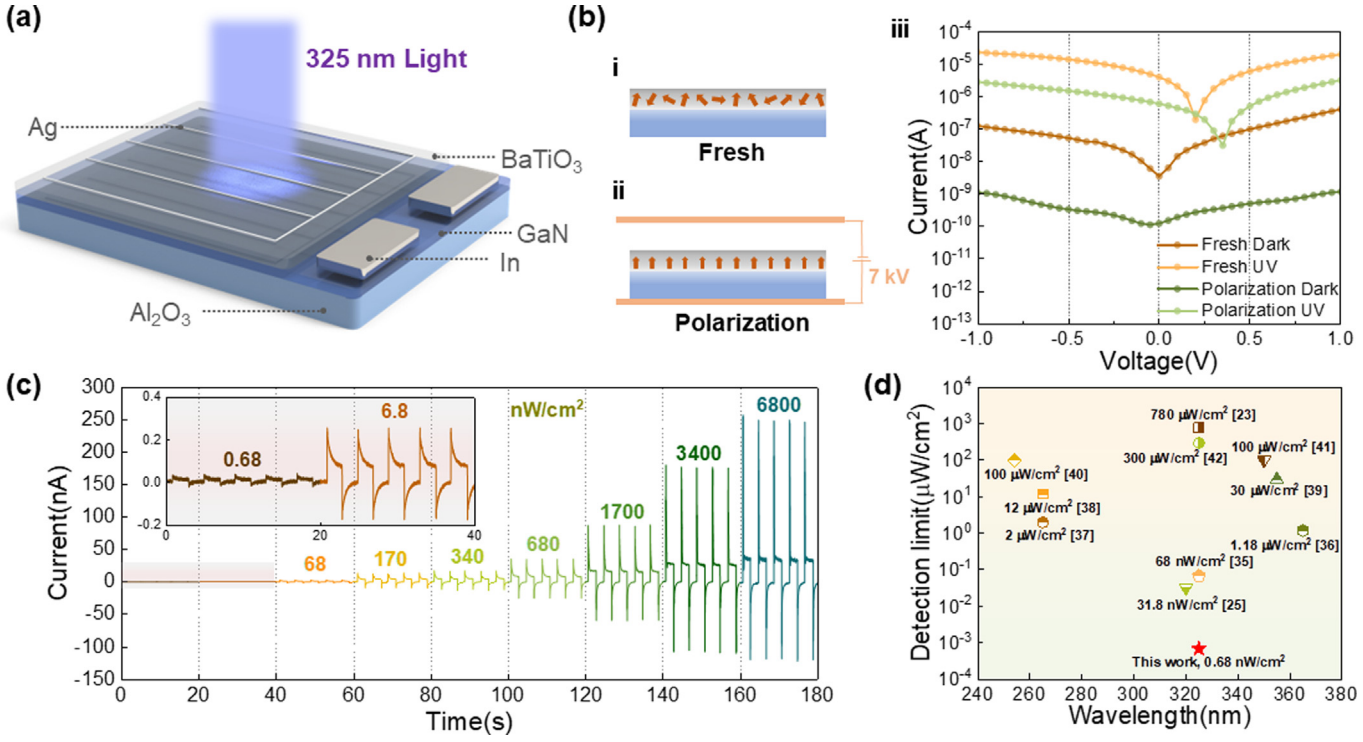

FIG. 3

Device structure and optoelectronic performance characterization. (a) Schematic diagram of device structure. (b) i. Schematic diagram of unpolarized device (Arrows represent ferroelectric domains within $BaTiO_3$ thin films). ii. Schematic diagram of polarized device. iii. I-V curves of the device before and after polarization under dark and light conditions. (c) I-t characteristics of polarized devices under different lighting conditions. (d) Comparison of detection limit between this work and other self-powered UV photodetectors.

Please cite this article in press as: M. Dong et al., Materials Today (2024), https://doi.org/10.1016/j.mattod.2024.03.004

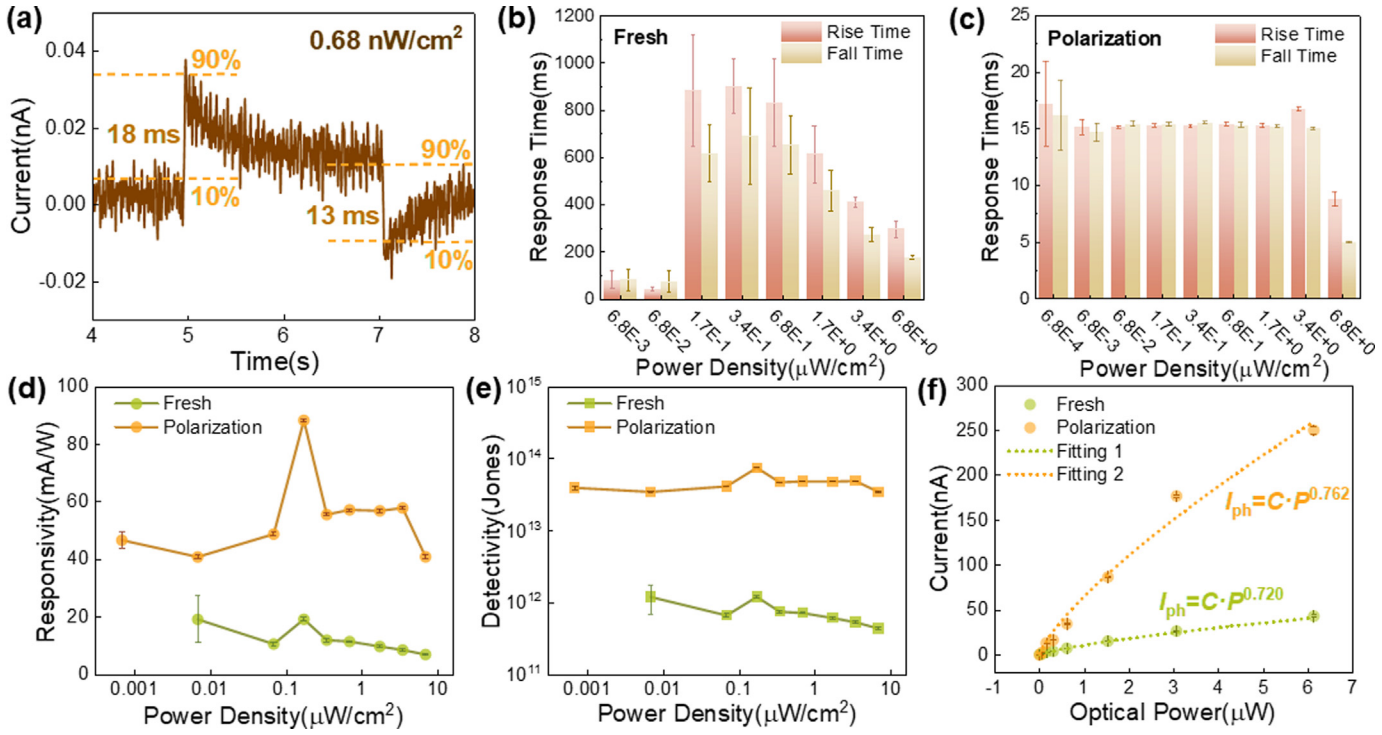

FIG. 4

Analysis of the photoresponse performance of the device. (a) Pulse time response analysis of a single photoelectric signal of the device under 0.68 nW/cm^2 incident light. Analysis of response time of the device in (b) fresh and (c) polarization state. (d) Responsivity, (e) detectivity, and (f) photocurrent peak of the device in fresh and polarization states.

polarization, the dark current of the device decreases by about two orders of magnitude, which will significantly reduce the noise current density of the device and enhance its detection performance against weak UV light [40]. However, due to the high residual polarization field provided by $BaTiO_3$ thin film blocking the diffusion of electrons, the photocurrent of the device also decreases. Fig. 3c shows the response of the polarized device to 325 nm UV light under different power densities. The photocurrent of the device consists of a pyroelectric current peak from $BaTiO_3$ thin film and a photocurrent platform from GaN thin film, and the photocurrent signal remains uniform under continuous incident light. As the intensity of incident light increases, the peak and platform of photocurrent also increase. This device has a sensitive response to ultra-weak UV light with an incident light power density of 0.68 nW/cm^2, which is currently the lowest detectable intensity by self-powered UV photodetectors (Fig. 3d) [11,29,31,41–48]. In contrast, unpolarized devices have high dark current and no response to the ultra-weak UV light of 0.68 nW/cm^2 (Fig. S9). And under weak UV light irradiation, the pyroelectric current is very small, displaying the poor response performance to weak UV light. The spectral responses of the device in the wavelength of 255, 265, 275, 295, 310, 360, 405, and 450 nm are shown in Fig. S10. The photocurrent is highest for the 360 nm light corresponding to the bandgap of the absorption layer GaN (~3.4 eV), whereas the photocurrent decreases sharply in under the illumination of the 405 nm or 450 nm light. The photocurrent in the 255–360 nm wavelength range decreases with the decrease of wavelength. This phenomenon is owing to the increased energy loss generated by high-energy light-induced hot electron relaxation [49]. As the incident light frequency increases, the response current of the device decreases and the waveform changes (Fig. S11). The response performance of the device decreases for frequency above 10 Hz, owing to the response speed of the device being in the ms level.

Analysis of the photoresponse performance of device

We detailly analyzed the photoresponse performance of the device, including response/recovery time, responsivity, detectivity, to demonstrate the ability to detect weak UV light. The device exhibits a fast response to ultra-weak UV light of 0.68 nW/cm^2, whose response/recovery time is 18 ms/13 ms (Fig. 4a). The fast response/recovery time is attributed to the pyroelectric spike current of $BaTiO_3$ and GaN thin film. The device in the fresh state responds faster to ultra-weak UV light of 68 nW/cm^2 and below (Fig. 4b), as the pyroelectric spike current is greater than the photocurrent platform at this power density of light. The response time of the pyroelectric current mainly determines the response speed of the device. Under the irradiation of UV light with a power density above 68 nW/cm^2, the photocurrent from GaN is greater than the pyroelectric current generated by $BaTiO_3$ thin film. The response time of the photocurrent platform limits the response speed of the device, resulting in a slower response to UV light. Moreover, due to the high level of dark current noise in unpolarized devices, their response to continuously incident UV light is uneven, resulting in a significant difference in response time and recovery time. After

Please cite this article in press as: M. Dong et al., Materials Today (2024), https://doi.org/10.1016/j.mattod.2024.03.004

polarization, the response speed of the device in the polarization state to UV light remains basically around 17 ms (Fig. 4c), which can achieve rapid light detection. This is because the pyroelectric spike current of the polarized device is always higher than the photocurrent platform at different optical power densities. Therefore, the response time and recovery time of the device are roughly the same. Under ultra-weak UV light irradiation of 0.68 nW/cm^2, the stability of photocurrent is greatly affected by dark current noise. Therefore, at this power density, the response time uniformity of the device to incident light is poor, but much better than that of the device in the fresh state. Responsivity and detectivity are important parameters for characterizing the performance of photodetectors. The responsivity and detectivity can be calculated using the following formula [50–52]:

$$R = \frac{I_P - I_D}{P}$$

$$D^* = \sqrt{\frac{A}{2eI_D}}R$$

where R represents responsivity, I_P represents photocurrent, I_D represents dark current, and P represents incident light power. D^* is the detectivity, A is the effective area of the device, and e is the amount of electron charge. Comparing the responsivity data of devices before and after polarization (Fig. 4d), it can be seen that the responsivity of devices in polarization state is more than twice that of devices in fresh state, and the devices in both states have the highest responsivity to incident light of 170 nW/cm^2, with 88.206 mA/W and 19.199 mA/W, respectively. Comparing the detectivity data of the devices before and after polarization (Fig. 4e), it can be seen that detectivity of the devices in polarization state is one order of magnitude higher than that of the devices before polarization, which is 7.392 × 10^{13} Jones and 1.199 × 10^{12} Jones under incident light of 170 nW/cm^2, respectively. The external quantum efficiency (EQE) represents the efficiency of the device in utilizing incident light. The EQE of devices before and after polarization can be obtained by the following formula [53]:

$$EQE = R\frac{hc}{e\lambda}$$

where h is the Planck constant, c is the speed of light, and λ is the wavelength of the incident light. As shown in Fig. S12, the external quantum efficiency of the device in polarization state is higher than that in fresh state, indicating that the polarization field improves the utilization of photons. This determines that the detection performance of the polarized device for weak UV

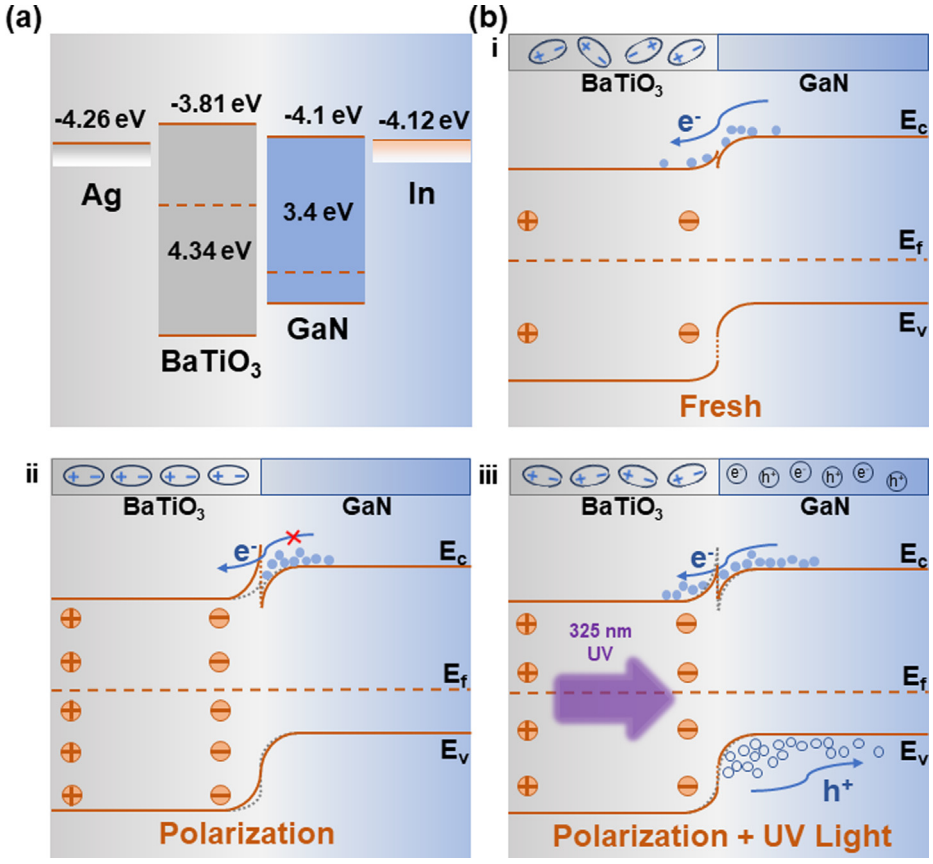

FIG. 5

The energy band structure of the device. (a) The energy band arrangement of Ag, $BaTiO_3$, GaN, In before contact. (b) i. Before polarization and ii after polarization the energy band arrangement of $BaTiO_3$/GaN heterojunction in the dark state. iii. Energy band arrangement of polarized $BaTiO_3$/GaN heterojunction under 325 nm UV light.

Please cite this article in press as: M. Dong et al., Materials Today (2024), https://doi.org/10.1016/j.mattod.2024.03.004

light is much better than that of the pre-polarized device. As shown in Fig. 4f, the photocurrent peaks of devices in polarization and fresh states were measured under different optical power densities of incident light, and fitted based on the power law relationship formula between photocurrent and incident light power [40]:

$$I_{ph} = C \cdot P^k$$

where I_{ph} represents photocurrent, C is a constant, P is the optical power, and k is the fitting parameter of photocurrent, representing the linearity of the photodetector. Here, in the polarization and fresh states, the fitted k-values are 0.762 and 0.720, respectively, showing a slight increase after polarization.

Physical mechanism of device performance

In order to explain the physical mechanism of ferroelectric field controlling device performance, we studied the contact potential barriers of all interfaces before and after polarization. Fig. 5a shows the initial band structures of the four materials, where an ohmic contact can be formed between the electrode and the semiconductor that is conducive to carrier transport. After the formation of $BaTiO_3$/GaN heterojunction, the energy band of $BaTiO_3$ bends upwards and the energy band of GaN bends downwards, forming a small potential barrier at the conduction band (Fig. 5b i). Due to the small potential barrier in the junction area, it is not sufficient to shield the hot electrons generated within the semiconductor. At this point, the source of dark current noise is carrier diffusion, and most high-energy electrons can cross the potential barrier and directly reach the surface of $BaTiO_3$, which is then collected by the Ag electrode to form a dark current. At this time, the level of dark current is relatively high. After high-voltage polarization of the device, the dipoles in the $BaTiO_3$ thin film are arranged neatly in the same direction (Fig. 5b ii). The negative polarization charge at the $BaTiO_3$/GaN heterojunction interface is significantly enhanced, which leads to an upward shift of the Fermi level on the $BaTiO_3$ surface [40], resulting in an upward bending of the energy band at the interface and the formation of a large potential barrier. The potential barrier of the conduction band effectively blocks the diffusion of charge carriers, and at this moment, the dark current is only formed

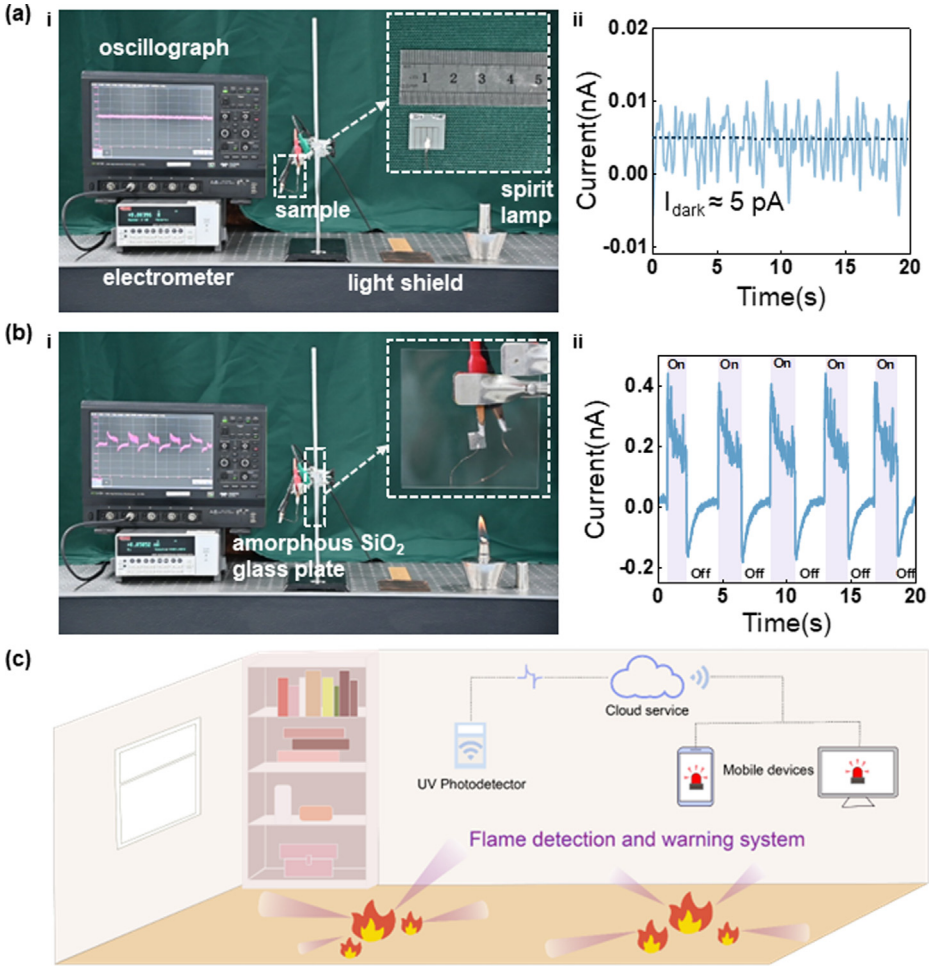

FIG. 6

The application of the device for flame detection. (a) i The experimental equipment used in the application demonstration, illustration is the optical image of the device. ii Dark current data of the device in dark state conditions. (b) i The ignited spirit lamp emits UV light onto the surface of the device, the illustration shows an amorphous SiO_2 glass plate used to block heat in front of the device. ii The photoelectric signal obtained by the device for flame detection. (c) Schematic diagram of the flame detection and warning system.

Please cite this article in press as: M. Dong et al., Materials Today (2024), https://doi.org/10.1016/j.mattod.2024.03.004

by a small portion of hot electron emissions, resulting in a significant reduction in the noise level of the dark current. When irradiated by UV light, the thermal effect generated will reduce the polarization intensity of $BaTiO_3$ thin film, thereby reducing the height of the potential barrier at the $BaTiO_3$/GaN heterojunction and weakening the blocking effect on electrons (Fig. 5b iii). The incidence of UV light will generate a large number of electron-hole pairs inside GaN, and under the action of potential barriers, the holes will diffuse towards the indium electrode direction, which will be collected by the electrode to form photocurrent. A small number of high-energy electrons will tunnel and reach the surface of $BaTiO_3$, which will be collected by the Ag electrode to form photocurrent. At the same time, the direction of ferroelectric domains in $BaTiO_3$ thin films changes due to UV light irradiation. The polarization intensity of the thin film decreases, resulting in the generation of a pyroelectric current (Fig. S13). Due to the upward polarization direction of $BaTiO_3$ thin film in the vertical direction, the pyroelectric spike current is consistent with the direction of photocurrent generated by GaN. Due to the influence of the residual polarization field, the height of the photocurrent platform of the polarized device has decreased, but the enhanced pyroelectric spike current effectively compensates for this disadvantage, allowing the device to have both ultra-low dark current and high spike photocurrent.

Application of device for flame detection

Based on the sensitive detection performance of the device to ultra-weak UV light, we further validated its application in flame detection. Fig. 6a i shows the equipment used in the experiment, and the illustration shows the optical image of the sample. Under dark state conditions, due to the presence of a ferroelectric field, the dark current of the device is extremely low, approximately 5 pA (Fig. 6a ii). The ignited spirit lamp will emit UV light, and at this time, the device is in a state of illumination, which will generate a photocurrent signal (Fig. 6b i). The illustration shows that there is an amorphous SiO_2 glass plate in front of the sample to block the heat generated by the flame, in order to avoid thermal energy causing the device to generate interference signal. Moving the light shield to simulate the generation of flames, the photocurrent data generated by the device is collected using an electrometer (Video S1), and the electrical signal shown in Fig. 6b ii is obtained. The waveform of the electrical signal generated by the flame is similar to that of the photoelectric signal generated by direct incidence of UV light, both consisting of pyroelectric peaks and photocurrent platforms. And the five consecutive electrical signals are highly uniform and have stable waveforms, proving that the device has excellent detection performance for flames. After 6 months of placement, the flame detection ability of the device is almost unchanged (Fig. S14), indicating excellent stability of the device. The components of the flame detection and warning system are shown in Fig. 6c. The UV photodetector receives UV light emitted by the flame, which generates an electrical signal. Electrical signals are transmitted wirelessly to cloud server for identification and storage, and then sent to mobile devices for remote monitoring and fire warning. The existence of flame detection and warning systems can greatly reduce the possibility of property damage and casualties caused by fires.

Conclusion

In summary, a self-powered $BaTiO_3$/GaN heterojunction UV photodetector for flame detection by coupling the ferroelectric polarization, anti-reflection effect, and pyro-phototronic effect is proposed and designed. $BaTiO_3$ thin films with a thickness of 20 nm is designed using the principle of destructive interference, resulting in a decrease in the reflectivity of the GaN thin film surface against 325 nm incident light from 21% to 12%, reducing the loss of incident light. The enhanced residual polarization field of polarized $BaTiO_3$ thin film has can regulate the energy band of $BaTiO_3$/GaN heterojunction, suppressing of the dark current and enhancing the pyroelectric current to improve the responsivity and detectivity of the device. The polarized device can stably detect ultra-weak UV light of 0.68 nW/cm^2, and the response time and recovery time of the device are as low as 18 ms and 13 ms, respectively. The maximum response and specific detection rates are 88.206 mA/W and 7.392×10^{13} Jones, respectively, increased by 359% and 6065% compared to the devices before polarization. It has a sensitive and stable response to continuously incident UV light. In addition, by simulating flame generation, it has been proven that the device has excellent performance in flame detection and can achieve remote monitoring and fire warning functions. Therefore, our research demonstrates that the presence of a ferroelectric field can significantly improve the weak light detection performance of $BaTiO_3$/GaN heterojunction photodetectors. At the same time, the coupling of pyroelectric current and photoelectric current synergistically enhances the sensitivity of the photodetector. $BaTiO_3$/GaN heterojunction photodetectors with ultra-weak UV light detection capabilities have a broad application potential in fields such as fire warning, ultraviolet guidance, and space communication.

CRediT authorship contribution statement

Mengji Dong: Writing – original draft, Investigation, Data curation. **Xuemei Zheng:** Data curation. **Qi Li:** Data curation. **Yanli Liu:** Data curation. **Xuan Di:** Data curation. **Jianping Meng:** Writing – review & editing, Writing – original draft, Supervision, Project administration, Methodology, Investigation, Funding acquisition, Data curation, Conceptualization. **Zhou Li:** Funding acquisition.

Data availability

The authors do not have permission to share data.

Declaration of competing interest

The authors declare that they have no known competing financial interests or personal relationships that could have appeared to influence the work reported in this paper.

Acknowledgements

The authors are thankful for the support provided by the National Natural Science Foundation of China (52002027, T2125003), the Youth Innovation Promotion Association CAS (2023175), the China Postdoctoral Science Foundation (119103S433), the Fundamental Research Funds for the Central Universities.

Please cite this article in press as: M. Dong et al., Materials Today (2024), https://doi.org/10.1016/j.mattod.2024.03.004

Appendix A. Supplementary data

Supplementary data to this article can be found online at https://doi.org/10.1016/j.mattod.2024.03.004.

References

[1] H. Chen et al., Mater. Today 18 (2015) 493–502.
[2] E. Monroy et al., Semicond. Sci. Technol. 18 (2003) R33–R51.
[3] S. Premi et al., Science 347 (2015) 842–847.
[4] H. Chen et al., Adv. Mater. 28 (2016) 403–433.
[5] Z. Li et al., Nat. Rev. Mater. 8 (2023) 587–603.
[6] H.P. Maruska, J. Tietjen, Appl. Phys. Lett. 15 (1969) 327–329.
[7] T. Lei et al., Appl. Phys. Lett. 59 (1991) 944–946.
[8] A. Dubey et al., Adv. Sci. 7 (2020) 2002274.
[9] S.K. Jain et al., ACS Appl. Electron. Mater. 3 (2021) 2407–2414.
[10] S. Kunwar et al., Nanomicro Lett. 12 (2020) 91.
[11] W. Song et al., Adv. Mater. 33 (2021) 2101059.
[12] S. Muhtadi et al., Appl. Phys. Express 10 (2017) 011004.
[13] A. Yoshikawa et al., Appl. Phys. Lett. 111 (2017) 191103.
[14] W. Tian et al., Small 13 (2017) 1701848.
[15] L.H. Zeng et al., Adv. Funct. Mater. 28 (2018) 1705970.
[16] L. Zeng et al., Nano Lett. 23 (2023) 8241–8248.
[17] H. Lin et al., Nanomaterials 12 (2022) 910.
[18] L. Su et al., Small 13 (2017) 1701687.
[19] L.H. Zeng et al., Adv. Sci. 6 (2019) 1901134.
[20] D. Guo et al., ACS Nano 12 (2018) 12827–12835.
[21] D. Wu et al., ACS Nano 13 (2019) 9907–9917.
[22] D. Wu et al., ACS Nano 16 (2022) 5545–5555.
[23] Y. Zhou et al., Nano Energy 100 (2022) 107516.
[24] M.F. Al Fattah et al., Nanoscale 13 (2021) 15526–15551.
[25] W. Ouyang et al., Appl. Phys. Rev. 8 (2021) 031315.
[26] X. Wang et al., Adv. Mater. 27 (2015) 6575–6581.
[27] Z. Dang et al., Nano Lett. 23 (2023) 6752–6759.
[28] L. Su et al., Adv. Funct. Mater. 33 (2023) 2214533.
[29] Y. Zhang et al., Nano Lett. 21 (2021) 8808–8816.
[30] S. Sahare et al., Nano Energy 107 (2023) 108172.
[31] L. Guo et al., ACS Nano 16 (2022) 1280–1290.
[32] Y. Ma et al., J. Mater. Chem. C 9 (2021) 881–887.
[33] Y. Liu et al., Small 18 (2022) 2106888.
[34] K.J. Choi et al., Science 306 (2004) 1005–1009.
[35] K. Zhao et al., iScience 3 (2018) 208–216.
[36] Ľ. Scholtz et al., Appl. Surf. Sci. 461 (2018) 249–254.
[37] L.V. Maneeshya et al., J. Mater. Sci. Mater. Electron. 26 (2015) 2947–2954.
[38] S. Al Kuhaimi, Vacuum 51 (1998) 349–355.
[39] H.K. Raut et al., Energy Environ. Sci. 4 (2011) 3779–3804.
[40] C. Jia et al., ACS Nano 17 (2023) 6534–6544.
[41] Q. Lu et al., Small 19 (2023) e2300364.
[42] J. Meng et al., Nano Today 43 (2022) 101399.
[43] S. Jiang et al., ACS Appl. Mater. Interfaces 14 (2022) 26279–26286.
[44] R. Zhuo et al., J. Mater. Chem. C 6 (2018) 299–303.
[45] R. Zhuo et al., Nano Res. 12 (2018) 183–189.
[46] Y. Wang et al., ACS Appl. Electron. Mater. 2 (2020) 2032–2038.
[47] J. Chen et al., ACS Appl. Mater. Interfaces 12 (2020) 53957–53965.
[48] W. Peng et al., Adv. Mater. 29 (2017) 1606698.
[49] C.A. Nelson et al., Energy Environ. Sci. 6 (2013) 3508–3519.
[50] D. Wu et al., Light Sci. Appl. 12 (2023) 5.
[51] L. Zeng et al., Adv. Mater. 32 (2020) 2004412.
[52] L.H. Zeng et al., Adv. Funct. Mater. 29 (2019) 1806878.
[53] D. Wu et al., ACS Nano 15 (2021) 10119–10129.

Please cite this article in press as: M. Dong et al., Materials Today (2024), https://doi.org/10.1016/j.mattod.2024.03.004